Journal of Structural Integrity and Maintenance

ISSN: (Print) (Online) Journal homepage: https://www.tandfonline.com/loi/tstr20

The optimum inertial amplifier viscoelastic base isolators for dynamic response mitigation of structures: an analytical study

Sudip Chowdhury, Arnab Banerjee & Sondipon Adhikari

To cite this article: Sudip Chowdhury, Arnab Banerjee & Sondipon Adhikari (2023) The optimum inertial amplifier viscoelastic base isolators for dynamic response mitigation of structures: an analytical study, Journal of Structural Integrity and Maintenance, 8:3, 150-160, DOI: 10.1080/24705314.2023.2176619

To link to this article: https://doi.org/10.1080/24705314.2023.2176619

JOURNAL OF STRUCTURAL INTEGRITY AND MAINTENANCE
2023, VOL. 8, NO. 3, 150–160
https://doi.org/10.1080/24705314.2023.2176619

Taylor & Francis
Taylor & Francis Group

The optimum inertial amplifier viscoelastic base isolators for dynamic response mitigation of structures: an analytical study

Sudip Chowdhury[a], Arnab Banerjee[a] and Sondipon Adhikari[b]

[a]Civil Engineering Department, Indian Institute of Technology Delhi (IITD), New Delhi, India; [b]James Watt School of Engineering, The University of Glasgow, Glasgow, Scotland, UK

ABSTRACT

The inertial amplifier viscoelastic base isolators (IAVBI) are introduced in this paper. The viscoelastic materials are implanted inside the core material of the inertial amplifier base isolators. The standard linear solid (SLS) models are applied to formulate the viscoelastic material mathematically. The viscoelastic materials are also implanted inside the traditional base isolators to enhance their dynamic response reduction capacity. The optimal dynamic responses of structures controlled by novel viscoelastic base isolators are derived analytically. The exact closed-form expressions for optimal design parameters of novel viscoelastic base isolators for structures are derived using H_2 and H_∞ optimization methods. The feasibility of these optimal design parameters has been tested by frequency domain analysis. The optimal dynamic response reduction capacity of inertial amplifier viscoelastic base isolators has been determined to investigate the robustness of the H_2 and H_∞ optimized design parameters. The closed-form expressions for optimal design parameters of novel base isolators are mathematically correct and effective for design purposes.

KEYWORDS

Inertial amplifier viscoelastic base isolators; traditional viscoelastic base isolators; standard linear solid; exact closed-form; H_2 and H_∞ optimization methods

Introduction

Base isolation mechanisms, together with the performance and different forms of the structure Aly and Salem (2013); Du et al. (2011); Ebrahimi et al. (2011); Wei et al. (2011), have been studied intensively since 1870 when the base isolation device was first discovered Touaillon (1870). Passive vibration control devices, such as vibration isolation bases and absorbers, have been installed in a wide variety of aeronautical, mechanical, and civil engineering structures, including vehicle suspensions Bai et al. (2017); Lindberg et al. (2014), liquid storage tanks Abal and Uckan (2010); X. Cheng et al. (2017), buildings Chowdhury et al. (2022a); Furinghetti et al. (2020, 2019, 2021); Mazza (2019); Sierra et al. (2019), bridges Sheng et al. (2022); Tubaldi et al. (2018), aircraft landing gear Han et al. (2019); de Haro Moraes et al. (2018), articulated towers D. C. Nguyen (2022), and nuclear power plant Tran et al. (2018) to control their dynamic responses Salman et al. (2020) subjected to earthquakes Minh Le et al. (2019), high wind pressure through the storm Pan et al. (2022). These isolation tools have widespread use in the building sector of civil engineering Jensen and Kusanovic (2014); Kim et al. (2016). To lessen the amplitude of resonant accelerations and inter-story drift Marian and Giaralis (2014), vibration isolation devices have been installed between the building's foundation and upper stories Hwang and Chiou (1996); Kazeminezhad et al. (2020); Tyapin (2016). There has also been nonlinear Chowdhury et al. (2022c) base isolation systems X. B. Nguyen et al. (2022), such as a New Zealand bearing Buckle (1985), a lead rubber bearing Robinson (1982), a resilient friction base isolator Jangid (2005a), a friction-pendulum system Jangid (2005b), and a pure-friction system Shakib and Fuladgar (2003); Su and Ahmadi (1988). It is common practice to employ H_2 optimization strategies Baduidana and Kenfack-Jiotsa (2021); Čakmak et al. (2021); Hu and Chen (2015) to construct closed-form equations for the optimum design Banerjee and Ghosh (2020) parameters of base isolation systems Asami et al. (2002); Z. Cheng et al. (2020); H. Sun et al. (2019). The controlled structures were randomly vibrated, and the standard deviation of the responses was reduced using the H_2 optimization Narkis and Lyrintzis (1994); Podworna et al. (2021) approach Crandall and Mark (2014); Palazzo and Petti (1999); Qian et al. (2019a); Roberts and Spanos (2003). However, when isolated structures are vibrated to harmonic excitations, the maximum dynamic responses of the main structures are minimized using H_∞ optimized isolators Allen (2012); Cheung and Wong (2011); Chun et al. (2015); Den Hartog (1985); Hua et al. (2018) effectively.

For example, mass amplification Chowdhury and Banerjee (2022a), negative stiffness, and negative mass, among other devices, have all been the subject of recent research into how they may be used to augment the effectiveness of existing vibration isolation methods Ayad, Karathanasopoulos, Ganghoffer, et al. (2020); Čakmak et al. (2022); Chen and Hu (2019); De Domenico et al. (2019); Jiang et al. (2020); Kuhnert et al. (2020); Moghimi and Makris (2020); Qian et al. (2019b); Smith and Wang (2004); F.-C. Wang et al. (2009); Zhang et al. (2019, 2018); Z. Zhao et al. (2019, 2020, 2020). Low-frequency effective mass amplification characteristics Chowdhury et al. (2023) have also been achieved using massive, wide-bandgap inertial amplifiers Ayad, Karathanasopoulos, Reda, et al. (2020); Barys et al. (2018); Barys and Zalewski (2018); Chowdhury et al. (2021, 2022b); Frandsen et al. (2016); Hou et al. (2017); Karathanasopoulos et al. (2020); Miniaci et al. (2020); Muhammad et al. (2020); F. Sun et al. (2021); Taniker and Yilmaz (2013, 2017); Yilmaz and Hulbert (2010, 2017); Yilmaz et al. (2007); Yuksel and Yilmaz (2015); Zhou et al. (2019). Magnetic negative stiffness dampers Shi and Zhu (2017); W. Wu et al. (2014), Euler buckled beams as negative

CONTACT Sudip Chowdhury sudip.chowdhury@civil.iitd.ac.in

stiffness components Fulcher et al. (2014); Huang et al. (2014); Liu et al. (2013); Winterflood et al. (2002); Yuan et al. (2021), pseudo-negative-stiffness Iemura et al. (2006); Iemura and Pradono (2009); Kapasakalis et al. (2020, 2021); M. Wang et al. (2018), and high-static-low-dynamic-stiffness Carrella et al. (2009, 2007); Hao and Cao (2015); Li et al. (2021); Robertson et al. (2009); F. Zhao et al. (2021) inclusions C. Cheng et al. (2016); J. Wu et al. (2022); Zheng et al. (2016) are all examples of negative stiffness devices. However, the current state of the art on isolation systems does not include using a viscoelastic material at the base isolator level to improve the system's overall vibration reduction capability or providing rigorous explicit analytical closed-form equations for the best possible design parameters. Most of the published works do not provide a closed-form formula but instead use contour plots to find the best possible outcomes.

The primary purpose of this work is to evaluate the efficiency of the inertial amplifier base viscoelastic isolators connected to a single degree of freedom system, thereby filling the aforementioned void in the literature. The standard linear model (SLS) has been applied to formulate the viscoelastic material mathematically. Closed-form equations for the optimal design parameters of the proposed base isolator are commonly derived using the H_2 and H_∞ optimization methods Chowdhury and Banerjee (2022b). To further ensure the correctness of the analytical closed-form equations for optimal design parameters, near-field earthquake ground movements were also analysed analytically in the frequency domain and numerically in the time domain.

Structural model and equations of motion

The mathematical diagram of single degree of freedom systems (SDOF) isolated by inertial amplifier viscoelastic base isolators (IAVBI) subjected to base excitation has been shown in Figure 1.

m_b and k_b define the mass and stiffness of IAVBI without the mass amplification effect of the inertial amplifier. c_b refers to the hereditary damping of IAVBI. k_v defines the stiffness of viscoelastic material. m_a refers to the mass of the inertial amplifier. θ refers to the inertial angle between the spring and the rigid links. x_g refers to the displacement of base excitation. m_s, k_s, and c_s refer to the mass, stiffness, and viscous damping of the main structure. u_s and u_b are the absolute displacement of Main structure and IAVBI. x_a and y_a refer to the displacement of amplifier's mass m_a in x and y-directions. m_{bv}, k_{bv}, and c_{bv} refer to the effective mass, stiffness, and viscous damping of the IAVBI with the mass amplification effect of the inertial amplifier and viscoelastic material k_{av} refers to the stiffness of the viscoelastic material after adding the effect of mass amplification effect of the inertial amplifier. k_{av} and c_{bv} represent the elastic and viscous damping property of viscoelastic material induced inside the inertial amplifier base isolators. These design parameters are also known as the storage coefficient and loss factor.

The mathematical model of inertial amplifier viscoelastic base isolators

An inertial amplifier viscoelastic base isolator with hereditary damping has been shown in Figure 1. Therefore, the equation of motion for the isolator has been derived as follows:

$$m_{bv}\ddot{x}_b + \Xi\dot{x}_b + k_{bv}x_b = -m_{bv}\ddot{x}_g \tag{1}$$

where $x_b = u_b - x_g$, defines the relative displacement of IAVBI w.r.t base. Ξ is the hereditary function and $\Xi\dot{x}_b$ has been solved by the convolution integral.

$$\Xi\dot{x}_b = \int_{-\infty}^{t} \Xi(t-\tau)\dot{x}_b(\tau)d\tau \tag{2}$$

It has been considered that the isolator is in the static condition at $t = 0$. Therefore, Equation (1) has been derived as

$$m_{bv}\ddot{x}_b + \int_{-\infty}^{t} \Xi(t-\tau)\dot{x}_b(\tau)d\tau + k_{bv}x_b = -m_{bv}\ddot{x}_g \tag{3}$$

The hereditary function Ξ can be expressed as, $\Xi(t) = k_{av}e^{-\frac{k_{av}t}{c_{bv}}}$ and the integrating form has Dirac function, $\Xi(t) = c_{bv}\delta$ at $k_{av} \to \infty$. The steady-state solutions are considered as $x_b = X_b e^{i\omega t}$ and $\ddot{x}_g = A_g e^{i\omega t}$. Therefore, the transfer function of Equation (3) has been derived as

$$X_b(\omega) = -\frac{m_{bv}}{\left[-\omega^2 m_{bv} + i\omega\Xi(\omega) + k_{bv}\right]^{-1}}A_g \tag{4}$$

$\Xi(\omega) = k_{av}c_{bv}/(i\omega c_{bv} + k_{av})$ has been substituted in Equation (4). Therefore, Equation (4) has been rewritten as

$$X_b(\omega) = -\frac{m_{bv}}{\left[-\omega^2 m_{bv} + \frac{i\omega k_{av}c_{bv}}{i\omega c_{bv} + k_{av}} + k_{bv}\right]^{-1}}A_g \tag{5}$$

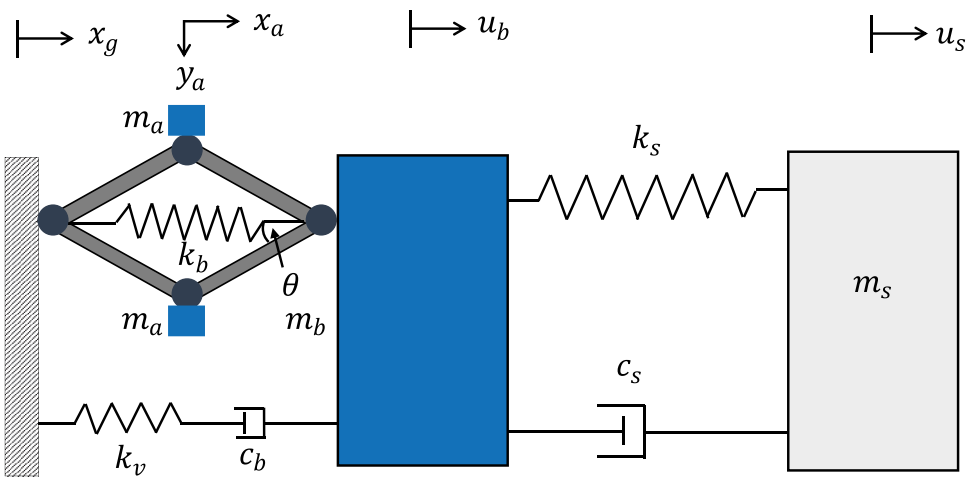

Figure 1. The schematic diagram of a single degree of freedom system isolated by inertial amplifier viscoelastic base isolators (IAVBI) subjected to base excitation.

Now, the derivation for effective mass amplification through the inertial amplifier has been performed to derive m_{bv}, c_{bv}, k_{bv}, and k_{av}. The deflections of amplifier's mass m_a in x and y-directions are derived as

$$x_a = \frac{u_b + x_g}{2} \quad \text{and} \quad y_a = \pm\frac{u_b - x_g}{2\tan\theta} \tag{6}$$

Therefore, the inertial forces developed through the amplifier's masses m_a in x and y- directions are derived as

$$p_x = m_a\ddot{x}_a \quad \text{and} \quad p_y = m_a\ddot{y}_a \tag{7}$$

The internal forces through the rigid links of the isolator have been derived as

$$p_1 = \frac{1}{2}\left(\frac{p_y}{\sin\theta} - \frac{p_x}{\cos\theta}\right) \quad \text{and} \quad p_2 = \frac{1}{2}\left(\frac{p_y}{\sin\theta} + \frac{p_x}{\cos\theta}\right) \tag{8}$$

The total resultant forces generated towards the end of the horizontal terminals are derived as

$$\begin{aligned} F &= 2p_2\cos\theta + k_b(u_b - x_g) \\ &= \underbrace{\frac{0.5m_a}{\tan^2\theta}}_{c1}(\ddot{u}_b - \ddot{x}_g) + \underbrace{0.5m_a}_{c2}(\ddot{u}_b + \ddot{x}_g) + k_{bv}(u_b - x_g) \end{aligned} \tag{9}$$

where $c_1 = (0.5m_a/\tan^2\theta)$ and $c_2 = 0.5m_a$ are the effective masses generated through the entire inertial amplifier and added to the base mass of the isolator m_b. Therefore, the total effective mass of the inertial amplifier viscoelastic base isolator has been derived as

$$m_{bv} = m_b + 0.5m_a\left(1 + \frac{1}{\tan^2\theta}\right) \tag{10}$$

The total effective stiffness for the inertial amplifier viscoelastic base isolator has been derived as

$$k_{bv} = m_{bv}\omega_b^2 \tag{11}$$

The total effective damping for inertial amplifier viscoelastic base isolator has been derived as

$$c_{bv} = 2\zeta_b m_{bv}\omega_b \tag{12}$$

The effective mass for the stiffness of viscoelastic material induced inside the IAVBI has been derived as

$$k_{av} = \kappa k_{bv} \tag{13}$$

where $\kappa = k_{av}/k_{bv}$ refers to the ratio of isolator stiffness to the viscoelastic material. The equations of motion of the main structure isolated by IAVBI subjected to base excitations have been derived and expressed as

$$\begin{aligned} m_{bv}\ddot{x}_b + \int_{-\infty}^{t}\Xi(t-\tau)\dot{x}_b(\tau)d\tau + k_{bv}x_b - k_s x_s - c_s\dot{x}_s &= -m_{bv}\ddot{x}_g \\ m_s\ddot{x}_s + m_s\ddot{x}_b + c_s\dot{x}_s + k_s x_s &= -m_s\ddot{x}_g \end{aligned} \tag{14}$$

The first equation of Equation (14) has also been derived as

$$\begin{aligned} m_{bv}\ddot{x}_b + \int_0^{\infty} k_{av}e^{-(k_{av}/c_{bv})(t-\tau)}\dot{x}_b(\tau)d\tau \\ + k_{bv}x_b - k_s x_s - c_s\dot{x}_s = -m_{bv}\ddot{x}_g \end{aligned} \tag{15}$$

where $x_b = u_b - x_g$ and $x_s = u_s - u_b$. The steady-state solutions for dynamic responses for isolated structures are determined as $x_s = X_s e^{i\omega t}$, $x_b = X_b e^{i\omega t}$, and $\ddot{x}_g = A_g e^{i\omega t}$. The viscous damping ratio of IAVBI has been defined as $\zeta_b = \frac{c_{bv}}{2\omega_b m_{bv}}$. The natural frequency of IAVBI is defined as $\omega_b = \sqrt{k_{bv}/m_{bv}}$. The ratio of base mass to the main structural mass is defined as $\mu_b = m_b/m_s$. The ratio of amplifier mass to the main structural mass is defined as $\mu_a = m_a/m_s$. The ratio of effective mass to main structural mass is defined as $\mu_{bv} = m_{bv}/m_s$. η_b defines the ratio of isolator frequency to the main structure's frequency. The stiffness of the main structure is defined as $k_s = \omega_s^2 m_s$. The viscous damping ratio of main structure defines as $\zeta_s = \frac{c_s}{2m_s\omega_s}$. The steady-state solutions and the design parameters are substituted in Equations (14) and (15). Therefore, the transfer function has been derived as

$$\left[\begin{pmatrix} 2\zeta_s q\omega_s + q^2 + {\omega_s}^2 & q^2 \\ -2\zeta_s q\omega_s - {\omega_s}^2 & \mu_{bv}q^2 + \frac{2q\kappa{\omega_b}^3{\mu_{bv}}^2\zeta_b}{\kappa\mu_{bv}{\omega_b}^2 + 2\mu_{bv}q\zeta_b\omega_b} + {\omega_b}^2\mu_{bv} \end{pmatrix}\right]\begin{Bmatrix} X_s \\ X_b \end{Bmatrix} = -\begin{bmatrix} -1 \\ -\mu_{bv} \end{bmatrix}A_g \tag{16}$$

Therefore, the dynamic response of the main structure has been derived as

$$H_s(q) = \frac{X_s}{A_g} = \frac{-2\kappa\mu_{bv}q\zeta_b{\omega_b}^2 - \kappa\omega_b\mu_{bv}{\omega_b}^2 - 2q\zeta_b\mu_{bv}{\omega_b}^2}{\Delta} \tag{17}$$

The dynamic response of IAVBI has been derived as

$$\begin{aligned} H_b(q) &= \frac{X_b}{A_g} \\ &= \frac{-(\kappa\omega_b + 2q\zeta_b)(2q\zeta_s\mu_{bv}\omega_s + \mu_{bv}q^2 + 2\zeta_s q\omega_s + \mu_{bv}{\omega_s}^2 + {\omega_s}^2)}{\Delta} \end{aligned} \tag{18}$$

Δ has been derived as

$$\begin{aligned} \Delta = {} & 2q^5\zeta_b\mu_{bv} + (4\zeta_b\zeta_s\mu_{bv}\omega_s + \kappa\omega_b\mu_{bv} + 4\zeta_b\zeta_s\omega_s)q^4 \\ & + \begin{pmatrix} 2\kappa\mu_{bv}\zeta_b{\omega_b}^2 + 2\kappa\omega_b\zeta_s\mu_{bv}\omega_s + 2\kappa\omega_b\zeta_s\omega_s \\ +2\zeta_b\mu_{bv}{\omega_b}^2 + 2\zeta_b\mu_{bv}{\omega_s}^2 + 2\zeta_b{\omega_s}^2 \end{pmatrix}q^3 \\ & + \begin{pmatrix} 4\kappa\mu_{bv}\zeta_b{\omega_b}^2\zeta_s\omega_s + 4\zeta_b\zeta_s\mu_{bv}{\omega_b}^2\omega_s + \kappa\omega_b\mu_{bv}{\omega_b}^2 \\ +\kappa\omega_b{\omega_s}^2\mu_{bv} + \kappa\omega_b{\omega_s}^2 \end{pmatrix}q^2 \\ & + (2\kappa\mu_{bv}\zeta_b{\omega_b}^2{\omega_s}^2 + 2\kappa\omega_b\zeta_s\mu_{bv}{\omega_b}^2\omega_s + 2\zeta_b\mu_{bv}{\omega_b}^2{\omega_s}^2)q \\ & + \kappa\omega_b\mu_{bv}{\omega_b}^2{\omega_s}^2 \end{aligned} \tag{19}$$

H_2 optimization for white-noise random excitation

H_2 optimization method has been applied to derive the closed-form expressions for optimal design parameters for IAVBI Chowdhury and Banerjee (2022b); Chowdhury et al.

(2022b). The viscous damping ratio of the main structure has been considered as $\zeta_s = 0$. Therefore, the standard deviation of the dynamic response of the main structure has been derived using Equations (17) and (19) and expressed as

$$\sigma_{x_s}^2 = \frac{S_0\omega_b\pi\left(\left(\left(4\mu_{bv}\zeta_b{}^2+1\right)\kappa^2+8\mu_{bv}\kappa\zeta_b{}^2+4\mu_{bv}\zeta_b{}^2\right)\omega_s{}^2+\kappa^2\mu_{bv}\omega_b{}^2\right)}{2\kappa^2\zeta_b\,\omega_s{}^6} \quad (20)$$

Equation (20) has been partially differentiated with respect to the viscous damping ratio ζ_b and natural frequency ω_b of IAVBI. Therefore, the mathematical equations for partial differentiation have been derived as

$$\frac{\partial\sigma_{x_s}^2}{\partial\zeta_b} = 0 \quad \text{and} \quad \frac{\partial\sigma_{x_s}^2}{\partial\omega_b} = 0 \quad (21)$$

Equation (20) has been substituted in the first equation of Eq. (21). Therefore, the closed-form expression for the viscous damping ratio of IAVBI has been derived as

$$\zeta_b = \frac{\sqrt{\mu_{bv}\left(\mu_{bv}\omega_b{}^2+\omega_s{}^2\right)}\kappa}{2\mu_{bv}\left(\kappa+1\right)\omega_s} \quad (22)$$

Equation (22) has been substituted in Equation (20). Therefore, the newly modified closed-form expression for the standard deviation of dynamic responses of the main structure has been derived as

$$\sigma_{x_s}^2 = \frac{2\pi\left(\mu_{bv}\omega_b{}^2+\omega_s{}^2\right)\omega_b S_0\mu_{bv}\left(\kappa+1\right)}{\omega_s{}^5\sqrt{\mu_{bv}\left(\mu_{bv}\omega_b{}^2+\omega_s{}^2\right)}\kappa} \quad (23)$$

Equation (23) has been substituted in the second equation of Equation (21). Therefore, the closed-form expression for the optimal frequency of IAVBI has been derived as

$$\left(\omega_b\right)_{opt} = \frac{\omega_s}{\sqrt{2\mu_{bv}}} \quad (24)$$

The non-dimensional form of Equation (24) has been derived as

$$\left(\eta_b\right)_{opt} = \frac{1}{\sqrt{2\mu_{bv}}}$$

where $\eta_b = \omega_b/\omega_s$ refers to the frequency ratio of IAVBI. Equation (24) has been substituted in Equations (22) and (23). Therefore, the optimal viscous damping ratio of IAVBI has been derived as

$$\left(\zeta_b\right)_{opt} = \frac{\sqrt{6}\sqrt{\mu_{bv}\omega_s{}^2}\kappa}{4\mu_{bv}\left(\kappa+1\right)\omega_s} \quad (26)$$

The variations of the optimal frequency ratio of IAVBI versus base mass ratio for different values of amplifier mass ratio have been shown in Figure 2(a). θ= 10^o has been considered for this graph. The optimal frequency ratio decreases when the base mass ratio and the amplifier's mass ratio increase.

The variations of the optimal frequency ratio of IAVBI versus base mass ratio for different values of the amplifier's inertial angle have been displayed in Figure 2(b). $\mu_a = 0.10$ has been considered for the amplifier's mass ratio. The frequency ratio increases when the amplifier's inertial angle increases and decreases when the base mass ratio increases. Therefore, a higher base mass ratio, a higher amplifier's mass ratio, and a lower inertial angle have been recommended to design an optimal IAVBI for enhancing the time period of the isolated structure during vibration. The variations of optimal viscous damping ratio of IAVBI versus base mass ratio for different values of amplifier's mass ratio have been displayed in Figure 3(a). $\kappa = 1$ has been considered for these graphs. The viscous damping ratio of IAVBI decreases when the base mass ratio and amplifier's mass ratio increase.

The variations of optimal viscous damping ratio of IAVBI versus base mass ratio for different values of the amplifier's inertial angle have been displayed in Figure 3(b). The viscous damping ratio increases when the inertial angle increases and decreases when the base mass ratio increases. The lower values of viscous damping for an isolator are cost-effective and smoothly implementable. Therefore, a higher base mass ratio, a higher amplifier's mass ratio, and a lower inertial angle are recommended for optimum IAVBI to achieve robust vibration reduction capacity at lower viscous damping.

H_∞ optimization for harmonic excitation

H_∞ optimization method has also been applied to derive the closed-form expressions for optimal design parameters of IAVBI Chowdhury et al. (2022b). The transfer function for the dynamic responses of the structure and IAVBI has been redefined as

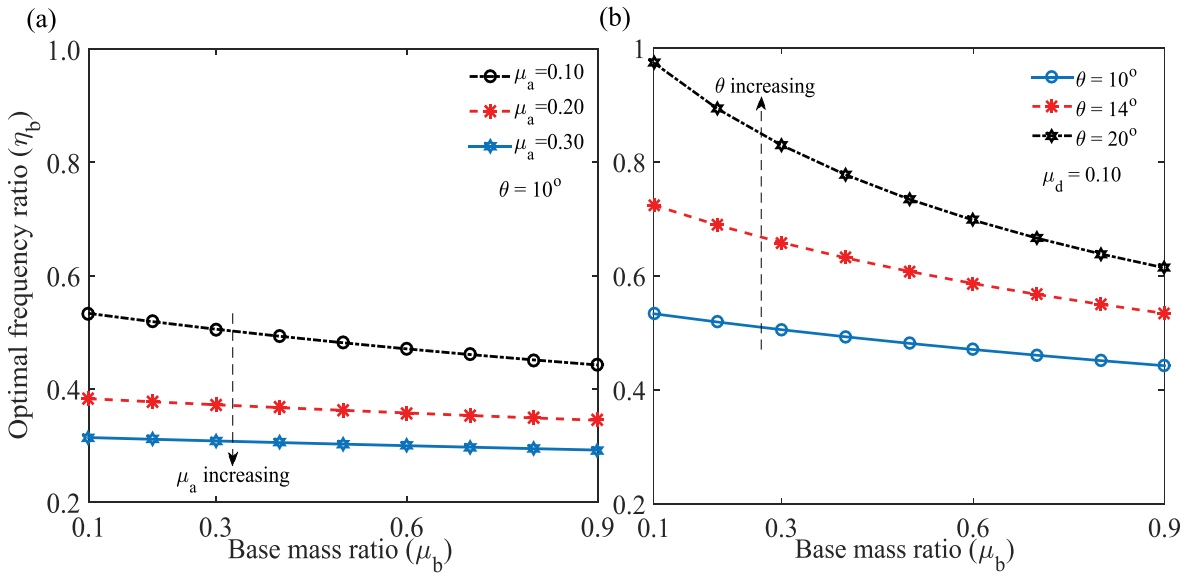

Figure 2. The variations of optimal frequency ratio versus base mass ratio for different values of (a) amplifier's mass ratio and (b) amplifier's inertial angle.

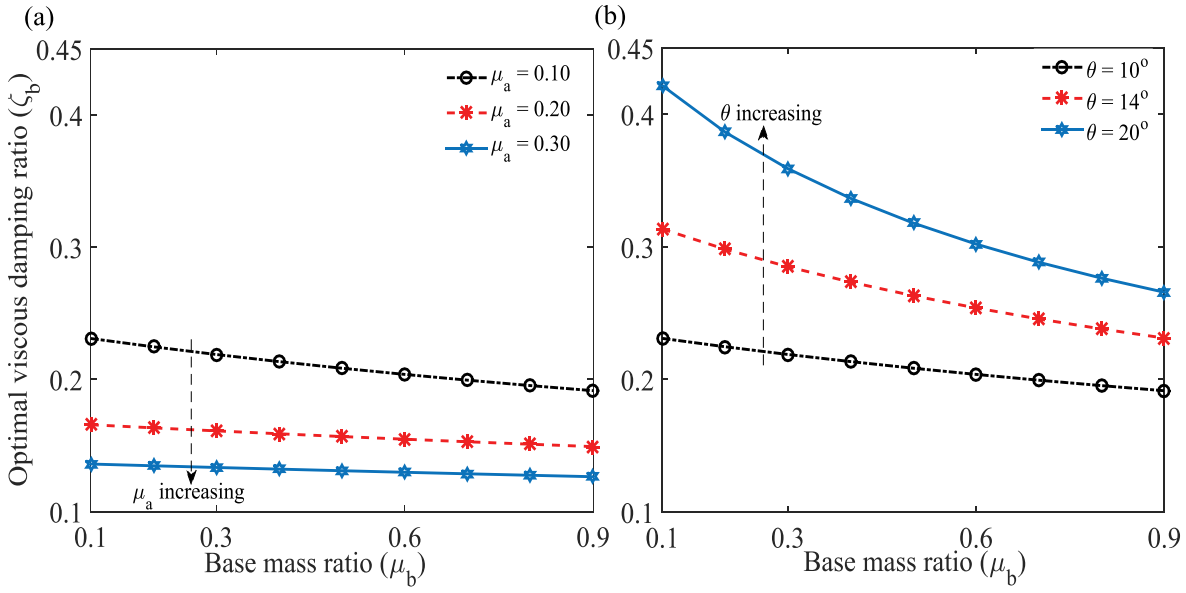

Figure 3. The variations of optimal viscous damping ratio versus base mass ratio for different values of (a) amplifier's mass ratio and (b) amplifier's inertial angle.

$$\begin{bmatrix} -\eta^2 + 2i\zeta_s\eta + 1 & -\eta^2 \\ -2i\zeta_s\eta - 1 & -\mu_{bv}\eta^2 + \frac{2i\eta\kappa\eta_b{}^3\mu_{bv}{}^2\zeta_b}{\kappa\eta_b{}^2\mu_{bv} + 2i\mu_{bv}\eta\,\eta_b\zeta_b} + \eta_b{}^2\mu_{bv} \end{bmatrix} \begin{Bmatrix} X_s \\ X_b \end{Bmatrix} = -\begin{bmatrix} 1 \\ \mu_{bv} \end{bmatrix} \frac{A_g}{\omega_s^2} \tag{27}$$

The dynamic response of the main structure has been derived as

$$H_s(\eta) = \frac{-\kappa\mu_{bv}\omega_b{}^3 - 2i\eta\mu_{bv}\omega_b{}^2\zeta_b(\kappa+1)}{\Delta} \tag{28}$$

The dynamic response of IAVBI has been derived as

$$H_b(\eta) = \frac{\eta^2\kappa\mu_{bv}\omega_b + 4\eta^2\zeta_b\zeta_s\mu_{bv} + 4\eta^2\zeta_b\zeta_s - \kappa\omega_b\mu_{bv} - \kappa\omega_b - 2i\eta\left((-\mu_{bv}\eta^2 + \mu_{bv} + 1)\zeta_b + \omega_b\kappa\zeta_s(\mu_{bv}+1)\right)}{\Delta} \tag{29}$$

Δ has been derived as

$$\Delta = \begin{matrix} -4\eta^2\kappa\mu_{bv}\omega_b{}^2\zeta_b\zeta_s + \eta^4\kappa\mu_{bv}\omega_b + 4\eta^4\mu_{bv}\zeta_b\zeta_s - \eta^2\kappa\mu_{bv}\omega_b{}^3 \\ -4\eta^2\mu_{bv}\omega_b{}^2\zeta_b\zeta_s + 4\eta^4\zeta_b\zeta_s - \eta^2\kappa\mu_{bv}\omega_b + \kappa\mu_{bv}\omega_b{}^3 - \eta^2\kappa\omega_b \\ +i\begin{pmatrix} -2\eta^3\kappa\mu_{bv}\omega_b{}^2\zeta_b + 2\eta^5\mu_{bv}\zeta_b - 2\eta^3\kappa\mu_{bv}\omega_b\zeta_s - 2\eta^3\mu_{bv}\omega_b{}^2\zeta_b \\ +2\eta\kappa\mu_{bv}\omega_b{}^3\zeta_s - 2\eta^3\kappa\omega_b\zeta_s + 2\eta\kappa\mu_{bv}\omega_b{}^2\zeta_b - 2\eta^3\zeta_b\mu_{bv} \\ +2\eta\mu_{bv}\omega_b{}^2\zeta_b - 2\eta^3\zeta_b \end{pmatrix} \end{matrix} \tag{30}$$

where $\eta = \omega/\omega_s$ refers to the ratio of excitation frequency to the main structure. $H_s(\eta)$ has been rewritten as

$$|H_s(\eta)| = \sqrt{\frac{A^2 + \zeta_b^2 B^2}{C^2 + \zeta_b^2 D^2}} = \left|\frac{B}{D}\right| \sqrt{\frac{\left(\frac{A}{B}\right)^2 + \zeta_b^2}{\left(\frac{C}{D}\right)^2 + \zeta_b^2}} \tag{31}$$

$$\begin{aligned} A &= -\kappa\mu_{bv}\eta_b{}^3 \\ B &= -2\eta\mu_{bv}\zeta_b\eta_b{}^2(\kappa+1) \\ C &= -4\eta^2\kappa\mu_{bv}\zeta_b\zeta_s\eta_b{}^2 + \eta^4\kappa\mu_{bv}\eta_b + 4\eta^4\mu_{bv}\zeta_b\zeta_s - \eta^2\kappa\mu_{bv}\eta_b{}^3 \\ &\quad - 4\eta^2\mu_{bv}\zeta_b\zeta_s\eta_b{}^2 + 4\eta^4\zeta_b\zeta_s - \eta^2\kappa\mu_{bv}\eta_b + \kappa\mu_{bv}\eta_b{}^3 - \eta^2\kappa\eta_b \\ D &= -2\eta^3\kappa\mu_{bv}\zeta_b\eta_b{}^2 + 2\eta^5\mu_{bv}\zeta_b - 2\eta^3\kappa\mu_{bv}\zeta_s\eta_b - 2\eta^3\mu_{bv}\zeta_b\eta_b{}^2 \\ &\quad + 2\eta\kappa\mu_{bv}\zeta_s\eta_b{}^3 - 2\eta^3\kappa\zeta_s\eta_b + 2\eta\kappa\mu_{bv}\zeta_b\eta_b{}^2 - 2\eta^3\zeta_b\mu_{bv} \\ &\quad + 2\eta\mu_{bv}\zeta_b\eta_b{}^2 - 2\eta^3\zeta_b \end{aligned} \tag{32}$$

From Equation (32), two constraint have been derived Chowdhury et al. (2022b); Den Hartog (1985) and expressed as

$$\left(\frac{A}{B}\right)^2\Big|_{\eta_j} = \left(\frac{C}{D}\right)^2\Big|_{\eta_j} \quad \text{and} \quad \left(\frac{B}{D}\right)^2\Big|_{\eta_1} = \left(\frac{B}{D}\right)^2\Big|_{\eta_2} \tag{33}$$

Considers $\zeta_s = 0$. Initially, the first constraint has been applied Chowdhury and Banerjee (2022b), and an equation has been derived. Therefore, the equation has been derived as

$$\begin{aligned} &(\mu_{bv}\kappa + 2\mu_{bv})\eta^4 + \left(-2\mu_{bv}\kappa\eta_b{}^2 - 2\mu_{bv}\eta_b{}^2 - \mu_{bv}\kappa - \kappa - 2\mu_{bv} - 2\right)\eta^2 \\ &\quad + 2\mu_{bv}\kappa\eta_b{}^2 + 2\mu_{bv}\eta_b{}^2 = 0 \\ &\text{and} \quad \eta_1^2 + \eta_2^2 = \frac{(2\kappa\eta_b{}^2 + 2\eta_b{}^2 + \kappa + 2)\mu_{bv} + \kappa + 2}{\mu_{bv}(\kappa+2)} \end{aligned} \tag{34}$$

The second equation of Equation (33) has been applied, and an equation has been derived. Therefore, the equation has been derived as

$$\begin{aligned} &-\mu_{bv}\eta_b{}^2(\kappa+1)(\eta_1 - \eta_2)(\eta_1 + \eta_2) \\ &\left(\mu_{bv}\kappa\eta_b{}^2 - \mu_{bv}\eta_1{}^2 - \mu_{bv}\eta_2{}^2 + \mu_{bv}\eta_b{}^2 + \mu_{bv} + 1\right) = 0 \\ &\text{and} \quad \eta_1^2 + \eta_2^2 = \frac{2\mu_{bv}\eta_b{}^2 + \mu_{bv} + 1}{\mu_{bv}}, \eta_1^2 + \eta_2^2 = 0, \eta_1^2 - \eta_2^2 = 0 \end{aligned} \tag{35}$$

Equations (34) and (35) are equating, and the closed-form expression for the optimal frequency ratio of IAVBI has been derived as

$$(\eta_b)_{opt} = \sqrt{\frac{\kappa\mu_{bv} + \kappa + 2\mu_{bv} + 2}{2\kappa\mu_{bv} + 2\mu_{bv}}} \tag{36}$$

The closed-form expression for $\eta_{1,2}^2$ has been derived as

$$\eta_{1,2}^2 = \pm\frac{\sqrt{2}\sqrt{(\kappa+2)(\kappa+1)\eta_b}}{\kappa+2} \tag{37}$$

Equation (36) has been substituted in Equation (37). Therefore, the closed-form expression for optimal $\eta_{1,2}^2$ has been derived as

$$(\eta_{1,2}^2)_{opt} = \pm\frac{\sqrt{(\kappa+2)(\kappa+1)}}{\kappa+2}\sqrt{\frac{(\mu_{bv}+1)(\kappa+2)}{\mu_{bv}(\kappa+1)}} \tag{38}$$

The mathematical expression for determining the closed-form expression for the optimal viscous damping ratio of IAVBI has been derived as

$$\frac{\partial|H_s(\eta)|^2}{\partial\eta^2}|_{\eta_{1,2}^2} = 0 \quad \text{and} \quad (\zeta_b)_{opt} = \sqrt{\frac{\zeta_{b1}^2+\zeta_{b2}^2}{2}} \tag{39}$$

The closed-form expression for the optimal damping ratio of IAVBI has been derived as

$$\begin{gathered} A\zeta_b^4 + B\zeta_b^2 + C = 0 \\ (\zeta_{b1,b2})_{opt}^2 = \left(\frac{-B\pm\sqrt{B^2-4AC}}{2A}\right)_{\eta_{1,2}} \end{gathered} \tag{40}$$

The coefficients of ζ_b are listed in Appendix A. The variations of the optimal frequency ratio of IAVBI as a function of base mass ratio and amplifier mass ratio have been shown in Figure 4(a). $\theta = 10^o$ has been considered for this graph. The optimal frequency ratio decreases when the base mass ratio and the amplifier's mass ratio increase.

The variations of the optimal frequency ratio of IAVBI as a function of base mass ratio and the amplifier's inertial angle have been displayed in Figure 4(b). $\mu_a = 0.10$ has been considered for the amplifier's mass ratio. The frequency ratio increases when the amplifier's inertial angle increases and decreases when the base mass ratio increases. Therefore, a higher base mass ratio, a higher amplifier's mass ratio, and a lower inertial angle have been recommended to design an optimal IAVBI for enhancing the time period of the isolated structure during vibration. The variation of optimal frequency ratio of H_∞ optimized IAVBI versus frequency ratio for different values of amplifier's mass ratio have been displayed in Figure 5(a). The optimal viscous damping ratio slightly increases as the base mass ratio and amplifier's mass ratio increase.

The variation of optimal frequency ratio of H_∞ optimized IAVBI versus frequency ratio for different values of amplifier's inertial angle have been displayed in Figure 5(b). The viscous damping ratio decreases as the inertial angle increases. However, small values of viscous damping ratio for viscoelastic isolators are made the total isolated structure under-damped. The dynamic response reduction capacity of IAVBI may decrease. Therefore, a higher base mass ratio, a higher amplifier's mass ratio, and lower inertial angles are recommended for designing H_∞ optimized IAVBI.

Robustness of H_2 and H_∞ optimized design parameters

The variations of optimal dynamic responses of main structures isolated by H_2 optimized IAVBI for different values of viscous damping ratio have been displayed in Figure 6(a). Equations (25) and (26) are applied to determine the optimal frequency and viscous damping ratio of H_2 optimized IAVBI. The other system parameters are considered as $\mu_b = 0.70$, $\mu_a = 0.10$, $\theta = 14^o$, $\kappa = 2.0$. The dynamic responses of the isolated structures are unrestrained for $\zeta_b = 0$, and the isolated structures are vibrated at their eigen frequencies, i.e. $\eta = 0.4255, 1.337$. The frequency points are shifted from its eigen frequencies when the viscous damping ratios increases, i.e. $\zeta_b \leq 1.0$. The maximum dynamic responses of main structures are minimized at the optimal frequency and viscous damping ratio points. Therefore, the resonating frequency points are determined as $\eta = 0.4403, 1.371$. The resonating frequency points are more shifted when the viscous damping ratios are increasing, i.e. $\zeta_b \geq 1.0$ and $\zeta_b = \infty$. The dynamic responses are also increasing infinitely. The frequency points are determined as $\eta = 0.6667, 1.471$. The optimal maximum dynamic response of the main structure has been determined as 3.16.

The variations of optimal dynamic responses of main structures isolated by H_∞ optimized IAVBI for different values of viscous damping ratio have been displayed in Figure 6(a).

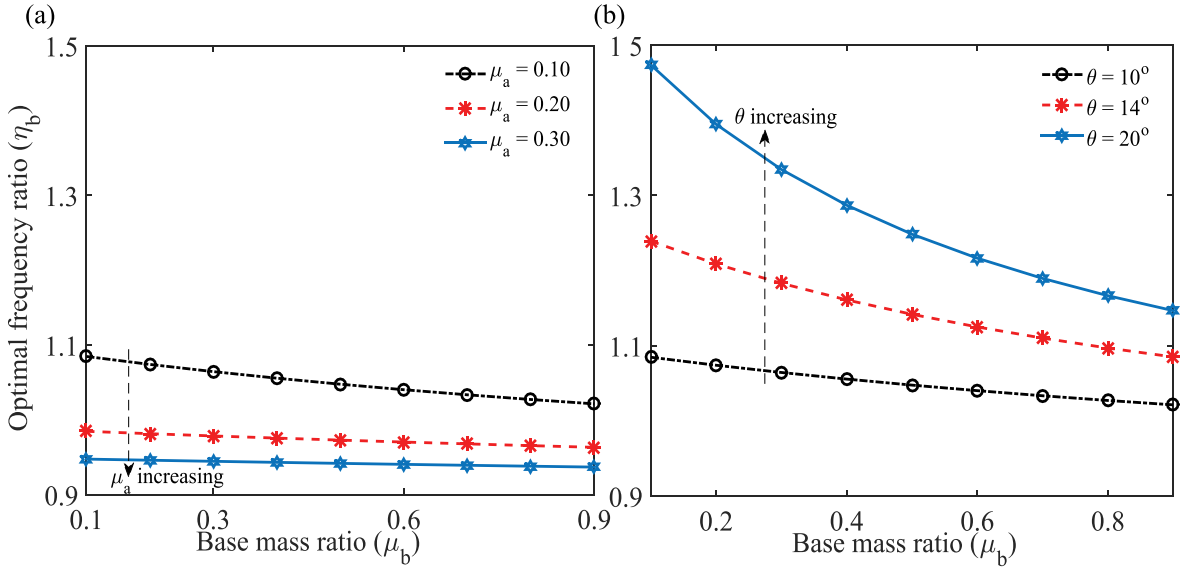

Figure 4. The variations of optimal frequency ratio versus base mass ratio for different values of (a) amplifier's mass ratio and (b) amplifier's inertial angle.

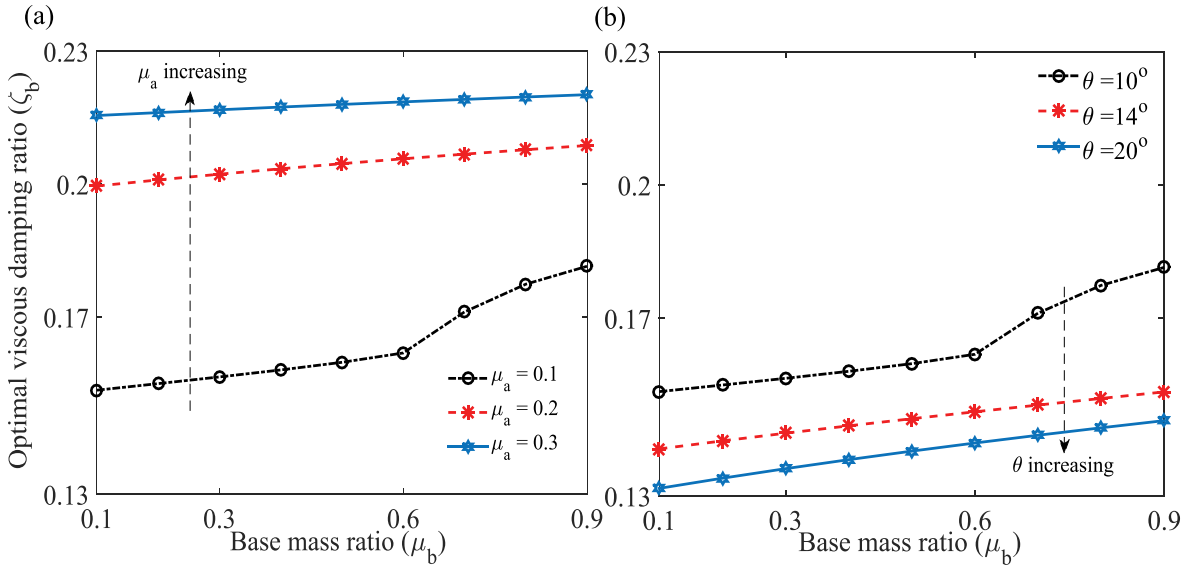

Figure 5. The variations of optimal viscous damping ratio versus base mass ratio for different values of (a) amplifier's mass ratio and (b) amplifier's inertial angle.

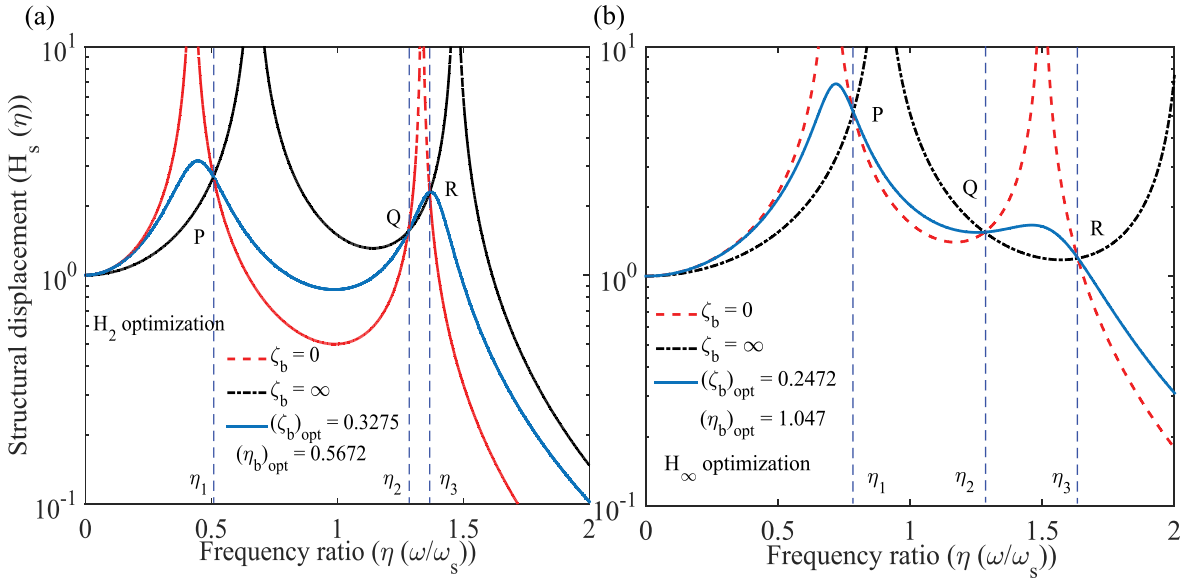

Figure 6. The variations of optimal dynamic responses of main structures versus frequency ratio for different values of viscous damping ratio of (a) H_2 and (b) H_∞ optimized IAVBI.

Equations (36) and (40) are applied to determine the optimal frequency and viscous damping ratio of H_∞ optimized IAVBI. The other system parameters are considered as $\mu_b = 0.70$, $\mu_a = 0.10$, $\theta = 14^o$, $\kappa = 2.0$. The dynamic responses of the isolated structures are unrestrained for $\zeta_b = 0$ and the isolated structures are vibrated at their eigen frequencies, i.e. $\eta = 0.7018, 1.504$. The frequency points are shifted from its eigen frequencies when the viscous damping ratios increases, i.e. $\zeta_b \leq 1.0$. The maximum dynamic responses of main structures are minimized at the optimal frequency and viscous damping ratio points. Therefore, the resonating frequency points are determined as $\eta = 0.7114, 1.49$. The resonating frequency points are more shifted when the viscous damping ratios are increasing, i.e. $\zeta_b \geq 1.0$ and $\zeta_b = \infty$. The dynamic responses are also increasing infinitely. The frequency points are determined as $\eta = 0.8865, 2.035$. The optimal maximum dynamic response of the main structure has been determined as 6.88. Therefore, The maximum dynamic responses of the isolated structures are lesser than the maximum dynamic responses of the uncontrolled structures. The effectiveness of the H_2 and H_∞ optimized design parameters are proven from these graphs. The results are mathematically accurate and feasible for practical design applications.

Summary and conclusions

The inertial amplifier viscoelastic base isolators (IAVBI) are introduced in this paper. H_2 and H_∞ optimization methods are applied to derive the closed-form expressions for optimal design parameters of IAVBI. A parametric study has been conducted with optimal closed-form expressions. The optimal dynamic responses of main structures isolated H_2 and H_∞ optimized IAVBI have been determined, and the robustness of these optimal closed-form expressions has been investigated. The significant outcomes are listed below.

- A higher base mass ratio, a higher amplifier's mass ratio and a lower inertial angle have been recommended to design H_2 optimized IAVBI for enhancing the time period of the isolated structure during vibration.

- A higher base mass ratio, a higher amplifier's mass ratio and a lower inertial angle are recommended for H_2 optimized IAVBI to achieve robust vibration reduction capacity at lower viscous damping.
- The trends of the H_∞ optimized frequency ratios are exactly same as H_2 optimized frequency ratio. A higher base mass ratio, a higher amplifier's mass ratio and a lower inertial angle have been recommended to design H_∞ optimized IAVBI for enhancing the time period of the isolated structure during vibration.
- The trends of the H_∞ optimized viscous damping ratios are exactly same as H_2 optimized viscous damping ratios. A higher base mass ratio, a higher amplifier's mass ratio and lower inertial angles are recommended for designing H_∞ optimized IAVBI for achieving robust dynamic response reduction capacity.
- The maximum dynamic responses of the isolated structures are lesser than the maximum dynamic responses of the uncontrolled structures. The effectiveness of the H_2 and H_∞ optimized design parameters are proven from these graphs. The results are mathematically accurate and feasible for practical design applications.

The novelty of the paper stands in introducing the inertial amplifier viscoelastic base isolators, which are not present in state-of-the-art based on the author's best knowledge. This paper produces many significant contributions. The proposition of the new closed-form expressions for optimal design parameters of the novel inertial amplifier viscoelastic base isolators is another significant contribution of this paper. These equations resulted in the optimal design of these novel isolators, resulting in the maximum amount of dynamic response reduction. These novel inertial amplifier viscoelastic base isolators are cost-effective. The practical realization, experimentation and prototyping of the proposed inertial amplifier viscoelastic base isolators will be the future scope of the research.

Acknowledgments

The authors would like to acknowledge the Inspire faculty grant, grant number DST/INSPIRE/04/2018/000052, for partial financial support for the project. SC would like to acknowledge the MHRD grant received from IIT Delhi during the period of this research work.

Disclosure statement

The authors declare that they have no known competing financial interests or personal relationships that could have appeared to influence the work reported in this paper.

Funding

The work was supported by the DST/ INSPIRE/INDIA [DST/ INSPIRE/04/2018/000052]; Indian Institute of Technology Delhi [MHRD Scholarship].

Data availability statement

All data, models, and code generated or used during the study appear in the submitted article. Data available within the article or its supplementary materials.

References

Abal, E., & Uckan, E. (2010). Parametric analysis of liquid storage tanks base isolated by curved surface sliding bearings. *Soil Dynamics and Earthquake Engineering*, *30*(1–2), 21–31. https://doi.org/10.1016/j.soildyn.2009.08.001

Allen, J. C. (2012). *H_∞ engineering and amplifier optimization*. Springer Science & Business Media.

Aly, A. A., & Salem, F. A. (2013). Vehicle suspension systems control: A review. *International Journal of Control, Automation, and Systems*, *2*(2), 46–54.

Asami, T., Nishihara, O., & Baz, A. M. (2002). Analytical solutions to h_∞ and h_2 optimization of dynamic vibration absorbers attached to damped linear systems. *Journal of Vibration and Acoustics*, *124*(2), 284–295. https://doi.org/10.1115/1.1456458

Ayad, M., Karathanasopoulos, N., Ganghoffer, J.-F., & Lakiss, H. (2020). Higher-gradient and micro-inertia contributions on the mechanical response of composite beam structures. *International Journal of Engineering Science*, *154*, 103318. https://doi.org/10.1016/j.ijengsci.2020.103318

Ayad, M., Karathanasopoulos, N., Reda, H., Ganghoffer, J.-F., & Lakiss, H. (2020). On the role of second gradient constitutive parameters in the static and dynamic analysis of heterogeneous media with micro-inertia effects. *International Journal of Solids and Structures*, *190*, 58–75. https://doi.org/10.1016/j.ijsolstr.2019.10.017

Baduidana, M., & Kenfack-Jiotsa, A. (2021). Optimal design of inerter-based isolators minimizing the compliance and mobility transfer function versus harmonic and random ground acceleration excitation. *Journal of Vibration and Control*, *27*(11–12), 1297–1310. https://doi.org/10.1177/1077546320940175

Bai, X.-X., Jiang, P., & Qian, L.-J. (2017). Integrated semi-active seat suspension for both longitudinal and vertical vibration isolation. *Journal of Intelligent Material Systems and Structures*, *28*(8), 1036–1049. https://doi.org/10.1177/1045389X16666179

Banerjee, S., & Ghosh, A. (2020). Optimal design of nonlinear TMD with Bingham-type damping for base-excited structures. *Journal of Structural Integrity and Maintenance*, *5*(4), 211–222. https://doi.org/10.1080/24705314.2020.1783121

Barys, M., Jensen, J. S., & Frandsen, N. M. (2018). Efficient attenuation of beam vibrations by inertial amplification. *European Journal of Mechanics-A/solids*, *71*, 245–257. https://doi.org/10.1016/j.euromechsol.2018.04.001

Barys, M., & Zalewski, R. (2018). Analysis of inertial amplification mechanism with smart spring-damper for attenuation of beam vibrations. *MATEC Web of Conferences*, 157, 03002. EDP Sciences.

Buckle, I. G. (1985). New Zealand seismic base isolation concepts and their application to nuclear engineering. *Nuclear Engineering and Design*, *84*(3), 313–326. https://doi.org/10.1016/0029-5493(85)90243-2

Čakmak, D., Tomičević, Z., Wolf, H., Božić, Ž., & Semenski, D. (2021). Stability and performance of supercritical inerter-based active vibration isolation systems. *Journal of Sound and Vibration*, *518*, 116234.

Čakmak, D., Tomičević, Z., Wolf, H., Božić, Ž., & Semenski, D. (2022). Stability and performance of supercritical inerter-based active vibration isolation systems. *Journal of Sound and Vibration*, *518*, 116234. https://doi.org/10.1016/j.jsv.2021.116234

Carrella, A., Brennan, M., Kovacic, I., & Waters, T. (2009). On the force transmissibility of a vibration isolator with quasi-zero-stiffness. *Journal of Sound and Vibration*, *322*(4–5), 707–717. https://doi.org/10.1016/j.jsv.2008.11.034

Carrella, A., Brennan, M., & Waters, T. (2007). Static analysis of a passive vibration isolator with quasi-zero-stiffness characteristic. *Journal of Sound and Vibration*, *301*(3–5), 678–689. https://doi.org/10.1016/j.jsv.2006.10.011

Cheng, X., Jing, W., & Gong, L. (2017). Simplified model and energy dissipation characteristics of a rectangular liquid-storage structure controlled with sliding base isolation and displacement-limiting devices. *Journal of Performance of Constructed Facilities*, *31*(5), 04017071. https://doi.org/10.1061/(ASCE)CF.1943-5509.0001066

Cheng, C., Li, S., Wang, Y., & Jiang, X. (2016). On the analysis of a high-static-low-dynamic stiffness vibration isolator with time-delayed cubic displacement feedback. *Journal of Sound and Vibration*, *378*, 76–91. https://doi.org/10.1016/j.jsv.2016.05.029

Cheng, Z., Palermo, A., Shi, Z., & Marzani, A. (2020). Enhanced tuned mass damper using an inertial amplification mechanism. *Journal of Sound and Vibration*, *475*, 115267. https://doi.org/10.1016/j.jsv.2020.115267

Chen, M. Z., & Hu, Y. (2019). *Inerter and its application in vibration control systems*. Springer.

Cheung, Y., & Wong, W. O. (2011). H-infinity optimization of a variant design of the dynamic vibration absorber—revisited and new results. *Journal of Sound and Vibration*, *330*(16), 3901–3912. https://doi.org/10.1016/j.jsv.2011.03.027

Chowdhury, S., & Banerjee, A. (2022a). The exact closed-form equations for optimal design parameters of enhanced inerter-based isolation systems. *Journal of Vibration and Control*, 10775463221133428. https://doi.org/10.1177/10775463221133428

Chowdhury, S., & Banerjee, A. (2022b). The exact closed-form expressions for optimal design parameters of resonating base isolators. *International Journal of Mechanical Sciences*, *224*, 107284. https://doi.org/10.1016/j.ijmecsci.2022.107284

Chowdhury, S., Banerjee, A., & Adhikari, S. (2021). Enhanced seismic base isolation using inertial amplifiers. *Structures*, *33*, 1340–1353. https://doi.org/10.1016/j.istruc.2021.04.089

Chowdhury, S., Banerjee, A., & Adhikari, S. (2022a). Optimal design of inertial amplifier base isolators for dynamic response control of multi-storey buildings. *International Journal of Structural Stability and Dynamics*. https://doi.org/10.1142/S0219455423500475

Chowdhury, S., Banerjee, A., & Adhikari, S. (2022b). Optimal negative stiffness inertial-amplifier-base-isolators: Exact closed-form expressions. *International Journal of Mechanical Sciences*, *218*, 107044. https://doi.org/10.1016/j.ijmecsci.2021.107044

Chowdhury, S., Banerjee, A., & Adhikari, S. (2022c). The optimum inertial amplifier tuned mass dampers for nonlinear dynamic systems. *International Journal of Applied Mechanics*, 2350009. https://doi.org/10.1142/S1758825123500096

Chowdhury, S., Banerjee, A., & Adhikari, S. (2023). The optimal design of dynamic systems with negative stiffness inertial amplifier tuned mass dampers. *Applied Mathematical Modelling*, *114*, 694–721. https://doi.org/10.1016/j.apm.2022.10.011

Chun, S., Lee, Y., & Kim, T.-H. (2015). h_∞ optimization of dynamic vibration absorber variant for vibration control of damped linear systems. *Journal of Sound and Vibration*, *335*, 55–65. https://doi.org/10.1016/j.jsv.2014.09.020

Crandall, S. H., & Mark, W. D. (2014). *Random vibration in mechanical systems*. Academic Press.

De Domenico, D., Deastra, P., Ricciardi, G., Sims, N. D., & Wagg, D. J. (2019). Novel fluid inerter based tuned mass dampers for optimised structural control of base-isolated buildings. *Journal of the Franklin Institute*, *356* (14), 7626–7649. https://doi.org/10.1016/j.jfranklin.2018.11.012

de Haro Moraes, F., Silveira, M., & Gonçalves, P. J. P. (2018). On the dynamics of a vibration isolator with geometrically nonlinear inerter. *Nonlinear Dynamics*, *93*(3), 1325–1340. https://doi.org/10.1007/s11071-018-4262-6

Den Hartog, J. P. (1985). *Mechanical vibrations*. Courier Corporation.

Du, H., Li, W., & Zhang, N. (2011). Semi-active variable stiffness vibration control of vehicle seat suspension using an mr elastomer isolator. *Smart Materials and Structures*, *20*(10), 105003. https://doi.org/10.1088/0964-1726/20/10/105003

Ebrahimi, B., Bolandhemmat, H., Khamesee, M. B., & Golnaraghi, F. (2011). A hybrid electromagnetic shock absorber for active vehicle suspension systems. *Vehicle System Dynamics*, *49*(1–2), 311–332. https://doi.org/10.1080/00423111003602400

Frandsen, N. M., Bilal, O. R., Jensen, J. S., & Hussein, M. I. (2016). Inertial amplification of continuous structures: Large band gaps from small masses. *Journal of Applied Physics*, *119*(12), 124902. https://doi.org/10.1063/1.4944429

Fulcher, B. A., Shahan, D. W., Haberman, M. R., Conner Seepersad, C., & Wilson, P. S. (2014). Analytical and experimental investigation of buckled beams as negative stiffness elements for passive vibration and shock isolation systems. *Journal of Vibration and Acoustics*, *136*(3). https://doi.org/10.1115/1.4026888

Furinghetti, M., Lanese, I., & Pavese, A. (2020). Experimental assessment of the seismic response of a base-isolated building through a hybrid simulation. *Recent Advances and Applications of Seismic Isolation and Energy Dissipation Devices*. https://doi.org/10.3389/fbuil.2020.00033

Furinghetti, M., Pavese, A., Quaglini, V., & Dubini, P. (2019). Experimental investigation of the cyclic response of double curved surface sliders subjected to radial and bidirectional sliding motions. *Soil Dynamics and Earthquake Engineering*, *117*, 190–202. https://doi.org/10.1016/j.soildyn.2018.11.020

Furinghetti, M., Yang, T., Calvi, P. M., & Pavese, A. (2021). Experimental evaluation of extra-stroke displacement capacity for curved surface slider devices. *Soil Dynamics and Earthquake Engineering*, *146*, 106752. https://doi.org/10.1016/j.soildyn.2021.106752

Han, C., Kang, B.-H., Choi, S.-B., Tak, J. M., & Hwang, J.-H. (2019). Control of landing efficiency of an aircraft landing gear system with magnetorheological dampers. *Journal of Aircraft*, *56*(5), 1980–1986. https://doi.org/10.2514/1.C035298

Hao, Z., & Cao, Q. (2015). The isolation characteristics of an archetypal dynamical model with stable-quasi-zero-stiffness. *Journal of Sound and Vibration*, *340*, 61–79. https://doi.org/10.1016/j.jsv.2014.11.038

Hou, M., Wu, J. H., Cao, S., Guan, D., & Zhu, Y. (2017). Extremely low frequency band gaps of beam-like inertial amplification metamaterials. *Modern Physics Letters B*, *31*(27), 1750251. https://doi.org/10.1142/S0217984917502517

Huang, X., Liu, X., Sun, J., Zhang, Z., & Hua, H. (2014). Vibration isolation characteristics of a nonlinear isolator using Euler buckled beam as negative stiffness corrector: A theoretical and experimental study. *Journal of Sound and Vibration*, *333*(4), 1132–1148. https://doi.org/10.1016/j.jsv.2013.10.026

Hua, Y., Wong, W., & Cheng, L. (2018). Optimal design of a beam-based dynamic vibration absorber using fixed-points theory. *Journal of Sound and Vibration*, *421*, 111–131. https://doi.org/10.1016/j.jsv.2018.01.058

Hu, Y., & Chen, M. Z. (2015). Performance evaluation for inerter-based dynamic vibration absorbers. *International Journal of Mechanical Sciences*, *99*, 297–307. https://doi.org/10.1016/j.ijmecsci.2015.06.003

Hwang, J., & Chiou, J. (1996). An equivalent linear model of lead-rubber seismic isolation bearings. *Engineering Structures*, *18*(7), 528–536. https://doi.org/10.1016/0141-0296(95)00132-8

Iemura, H., Igarashi, A., Pradono, M. H., & Kalantari, A. (2006). Negative stiffness friction damping for seismically isolated structures. *Structural Control and Health Monitoring: The Official Journal of the International Association for Structural Control and Monitoring and of the European Association for the Control of Structures*, *13*(2–3), 775–791. https://doi.org/10.1002/stc.111

Iemura, H., & Pradono, M. H. (2009). Advances in the development of pseudo-negative-stiffness dampers for seismic response control. *Structural Control and Health Monitoring: The Official Journal of the International Association for Structural Control and Monitoring and of the European Association for the Control of Structures*, *16*, 784–799. https://doi.org/10.1002/stc.345

Jangid, R. (2005a). Computational numerical models for seismic response of structures isolated by sliding systems. *Structural Control & Health Monitoring*, *12*(1), 117–137. https://doi.org/10.1002/stc.59

Jangid, R. (2005b). Optimum friction pendulum system for near-fault motions. *Engineering Structures*, *27*(3), 349–359. https://doi.org/10.1016/j.engstruct.2004.09.013

Jensen, H. A., & Kusanovic, D. (2014). On the effect of near-field excitations on the reliability-based performance and design of base-isolated structures. *Probabilistic Engineering Mechanics*, *36*, 28–44. https://doi.org/10.1016/j.probengmech.2014.03.003

Jiang, Y., Zhao, Z., Zhang, R., De Domenico, D., & Pan, C. (2020). Optimal design based on analytical solution for storage tank with inerter isolation system. *Soil Dynamics and Earthquake Engineering*, *129*, 105924. https://doi.org/10.1016/j.soildyn.2019.105924

Kapasakalis, K. A., Antoniadis, I. A., & Sapountzakis, E. J. (2020). Performance assessment of the kdamper as a seismic absorption base. *Structural Control & Health Monitoring*, *27*(4), e2482. https://doi.org/10.1002/stc.2482

Kapasakalis, K. A., Antoniadis, I. A., & Sapountzakis, E. J. (2021). Constrained optimal design of seismic base absorbers based on an extended kdamper concept. *Engineering Structures*, *226*, 111312. https://doi.org/10.1016/j.engstruct.2020.111312

Karathanasopoulos, N., Dos Reis, F., Diamantopoulou, M., & Ganghoffer, J.-F. (2020). Mechanics of beams made from chiral metamaterials: Tuning deflections through normal-shear strain couplings. *Materials & Design*, *189*, 108520. https://doi.org/10.1016/j.matdes.2020.108520

Kazeminezhad, E., Kazemi, M. T., & Mirhosseini, S. M. (2020). Assessment of the vertical stiffness of elastomeric bearing due to displacement and rotation. *International Journal of Non-Linear Mechanics*, *119*, 103306. https://doi.org/10.1016/j.ijnonlinmec.2019.103306

Kim, D., Wang, F., & Chaudhary, S. (2016). Modal energy balance approach for seismic performance evaluation of building structures considering

nonlinear behaviour. *Journal of Structural Integrity and Maintenance*, *1* (1), 10–17. https://doi.org/10.1080/24705314.2016.1153309

Kuhnert, W. M., Gonçalves, P. J. P., Ledezma-Ramirez, D. F., & Brennan, M. J. (2020). Inerter-like devices used for vibration isolation: A historical perspective. *Journal of the Franklin Institute*, *358*(1), 1070–1086. https://doi.org/10.1016/j.jfranklin.2020.11.007

Li, M., Cheng, W., & Xie, R. (2021). A quasi-zero-stiffness vibration isolator using a cam mechanism with user-defined profile. *International Journal of Mechanical Sciences*, *189*, 105938. https://doi.org/10.1016/j.ijmecsci.2020.105938

Lindberg, E., Östberg, M., Hörlin, N.-E., & Göransson, P. (2014). A vibro-acoustic reduced order model using undeformed coupling interface substructuring–application to rubber bushing isolation in vehicle suspension systems. *Applied Acoustics*, *78*, 43–50. https://doi.org/10.1016/j.apacoust.2013.11.001

Liu, X., Huang, X., & Hua, H. (2013). On the characteristics of a quasi-zero stiffness isolator using Euler buckled beam as negative stiffness corrector. *Journal of Sound and Vibration*, *332*(14), 3359–3376. https://doi.org/10.1016/j.jsv.2012.10.037

Marian, L., & Giaralis, A. (2014). Optimal design of a novel tuned mass-damper–inerter (tmdi) passive vibration control configuration for stochastically support-excited structural systems. *Probabilistic Engineering Mechanics*, *38*, 156–164. https://doi.org/10.1016/j.probengmech.2014.03.007

Mazza, F. (2019). Effects of the long-term behaviour of isolation devices on the seismic response of base-isolated buildings. *Structural Control & Health Monitoring*, *26*(4), e2331. https://doi.org/10.1002/stc.2331

Minh Le, L., Van Nguyen, D., Chang, S., Kim, D., Cho, S. G., & Nguyen, D. D. (2019). Vibration control of jacket offshore wind turbine subjected to earthquake excitations by using friction damper. *Journal of Structural Integrity and Maintenance*, *4*(1), 1–5. https://doi.org/10.1080/24705314.2019.1565055

Miniaci, M., Mazzotti, M., Amendola, A., & Fraternali, F. (2020). Inducing dispersion curves with negative group velocity in inertially amplified phononic crystals through the application of an external state of prestress. In *XI International Conference on Structural Dynamic, EURODYN 2020* (pp. 612–620).

Moghimi, G., & Makris, N. (2020). Seismic response of yielding structures equipped with inerters. *Soil Dynamics and Earthquake Engineering*, *141*, 106474. https://doi.org/10.1016/j.soildyn.2020.106474

Muhammad, S., Wang, S., Li, F., & Zhang, C. (2020). Bandgap enhancement of periodic nonuniform metamaterial beams with inertial amplification mechanisms. *Journal of Vibration and Control*, *26*(15–16), 1077546319895630. https://doi.org/10.1177/1077546319895630

Narkis, Y., & Lyrintzis, C. S. (1994). Optimal isolation and response of a linear-quadratic system under random excitation. *Probabilistic Engineering Mechanics*, *9*(3), 213–219. https://doi.org/10.1016/0266-8920(94)90007-8

Nguyen, D. C. (2022). Vibration control of an articulated tower with a tuned mass damper subjected to the inertial force of ground acceleration. *Journal of Structural Integrity and Maintenance*, *7*(3), 188–197. https://doi.org/10.1080/24705314.2022.2048240

Nguyen, X. B., Komatsuzaki, T., & Truong, H. T. (2022). Adaptive parameter identification of bouc-wen hysteresis model for a vibration system using magnetorheological elastomer. *International Journal of Mechanical Sciences*, *213*, 106848. https://doi.org/10.1016/j.ijmecsci.2021.106848

Palazzo, B., & Petti, L. (1999). Optimal structural control in the frequency domain: Control in norm H2 and H∞. *Journal of Structural Control*, *6*(2), 205–221. https://doi.org/10.1002/stc.4300060202

Pan, Z., Wang, W., Li, X., Chen, F., & Jiang, Z. (2022). Passive control of feather fault offshore wind turbine under combined earthquake wind and wave loads. *Journal of Structural Integrity and Maintenance*, *7*(2), 75–90. https://doi.org/10.1080/24705314.2021.2018842

Podworna, M., Sniady, P., & Grosel, J. (2021). Random vibrations of a structure modified by damped absorbers. *Probabilistic Engineering Mechanics*, *66*, 103151. https://doi.org/10.1016/j.probengmech.2021.103151

Qian, F., Luo, Y., Sun, H., Tai, W. C., & Zuo, L. (2019a). Optimal tuned inerter dampers for performance enhancement of vibration isolation. *Engineering Structures*, *198*, 109464. https://doi.org/10.1016/j.engstruct.2019.109464

Qian, F., Luo, Y., Sr., Sun, H., Tai, W. C., & Zuo, L. (2019b). Performance enhancement of a base-isolation structure using optimal tuned inerter dampers. *Active and Passive Smart Structures and Integrated Systems XIII*, 10967, 1096715. International Society for Optics and Photonics.

Robertson, W. S., Kidner, M., Cazzolato, B. S., & Zander, A. C. (2009). Theoretical design parameters for a quasi-zero stiffness magnetic spring for vibration isolation. *Journal of Sound and Vibration*, *326*(1–2), 88–103. https://doi.org/10.1016/j.jsv.2009.04.015

Roberts, J. B., & Spanos, P. D. (2003). *Random vibration and statistical linearization*. Courier Corporation.

Robinson, W. H. (1982). Lead-rubber hysteretic bearings suitable for protecting structures during earthquakes. *Earthquake Engineering & Structural Dynamics*, *10*(4), 593–604. https://doi.org/10.1002/eqe.4290100408

Salman, K., Kim, D., Maher, A., & Latif, A. (2020). Optimal control on structural response using outrigger braced frame system under lateral loads. *Journal of Structural Integrity and Maintenance*, *5*(1), 40–50. https://doi.org/10.1080/24705314.2019.1701799

Shakib, H., & Fuladgar, A. (2003). Response of pure-friction sliding structures to three components of earthquake excitation. *Computers & Structures*, *81*(4), 189–196. https://doi.org/10.1016/S0045-7949(02)00444-3

Sheng, T., Liu, G.-B., Bian, X.-C., Shi, W.-X., & Chen, Y. (2022). Development of a three-directional vibration isolator for buildings subject to metro-and earthquake-induced vibrations. *Engineering Structures*, *252*, 113576. https://doi.org/10.1016/j.engstruct.2021.113576

Shi, X., & Zhu, S. (2017). Simulation and optimization of magnetic negative stiffness dampers. *Sensors and Actuators A: Physical*, *259*, 14–33. https://doi.org/10.1016/j.sna.2017.03.026

Sierra, I. E. M., Losanno, D., Strano, S., Marulanda, J., & Thomson, P. (2019). Development and experimental behavior of hdr seismic isolators for low-rise residential buildings. *Engineering Structures*, *183*, 894–906. https://doi.org/10.1016/j.engstruct.2019.01.037

Smith, M. C., & Wang, F.-C. (2004). Performance benefits in passive vehicle suspensions employing inerters. *Vehicle System Dynamics*, *42*(4), 235–257. https://doi.org/10.1080/00423110412331289871

Su, L., & Ahmadi, G. (1988). Response of frictional base isolation systems to horizontal-vertical random earthquake excitations. *Probabilistic Engineering Mechanics*, *3*(1), 12–21. https://doi.org/10.1016/0266-8920(88)90003-3

Sun, F., Dai, X., Liu, Y., & Xiao, L. (2021). Seismic mitigation performance of periodic foundations with inertial amplification mechanism considering superstructure-foundation interaction. *Smart Materials and Structures*, *30*(2), 025018. https://doi.org/10.1088/1361-665X/abd58e

Sun, H., Zuo, L., Wang, X., Peng, J., & Wang, W. (2019). Exact h2 optimal solutions to inerter-based isolation systems for building structures. *Structural Control & Health Monitoring*, *26*(6), e2357. https://doi.org/10.1002/stc.2357

Taniker, S., & Yilmaz, C. (2013). Phononic gaps induced by inertial amplification in bcc and FCC lattices. *Physics Letters A*, *377*(31–33), 1930–1936. https://doi.org/10.1016/j.physleta.2013.05.022

Taniker, S., & Yilmaz, C. (2017). Generating ultra wide vibration stop bands by a novel inertial amplification mechanism topology with flexure hinges. *International Journal of Solids and Structures*, *106*, 129–138. https://doi.org/10.1016/j.ijsolstr.2016.11.026

Touaillon, J. (1870). Improvement in buildings. *U.S. Patent No. 99,973*.

Tran, T.-T., Nguyen, T.-H., & Kim, D. (2018). Seismic incidence on base-isolated nuclear power plants considering uni-and bi-directional ground motions. *Journal of Structural Integrity and Maintenance*, *3*(2), 86–94. https://doi.org/10.1080/24705314.2018.1461547

Tubaldi, E., Mitoulis, S. A., & Ahmadi, H. (2018). Comparison of different models for high damping rubber bearings in seismically isolated bridges. *Soil Dynamics and Earthquake Engineering*, *104*, 329–345. https://doi.org/10.1016/j.soildyn.2017.09.017

Tyapin, A. G. (2016). Damping in the platform models for soil-structure interaction problems: Rayleigh damping options and limitations in modal analysis. *Journal of Structural Integrity and Maintenance*, *1*(3), 114–123. https://doi.org/10.1080/24705314.2016.1211237

Wang, F.-C., Liao, M.-K., Liao, B.-H., Su, W.-J., & Chan, H.-A. (2009). The performance improvements of train suspension systems with mechanical networks employing inerters. *Vehicle System Dynamics*, *47*(7), 805–830. https://doi.org/10.1080/00423110802385951

Wang, M., Sun, F.-F., & Jin, H.-J. (2018). Performance evaluation of existing isolated buildings with supplemental passive pseudo-negative stiffness devices. *Engineering Structures*, *177*, 30–46. https://doi.org/10.1016/j.engstruct.2018.09.049

Wei, X., Lui, H., & Qin, Y. (2011). Fault isolation of rail vehicle suspension systems by using similarity measure. In *Proceedings of 2011 IEEE*

International Conference on Service Operations, Logistics and Informatics (pp. 391–396). IEEE.

Winterflood, J., Blair, D. G., & Slagmolen, B. (2002). High performance vibration isolation using springs in Euler column buckling mode. *Physics Letters A*, *300*(2–3), 122–130. https://doi.org/10.1016/S0375-9601(02)00258-X

Wu, W., Chen, X., & Shan, Y. (2014). Analysis and experiment of a vibration isolator using a novel magnetic spring with negative stiffness. *Journal of Sound and Vibration*, *333*(13), 2958–2970. https://doi.org/10.1016/j.jsv.2014.02.009

Wu, J., Zeng, L., Han, B., Zhou, Y., Luo, X., Li, X., Chen, X., & Jiang, W. (2022). Analysis and design of a novel arrayed magnetic spring with high negative stiffness for low-frequency vibration isolation. *International Journal of Mechanical Sciences*, *216*, 106980. https://doi.org/10.1016/j.ijmecsci.2021.106980

Yilmaz, C., & Hulbert, G. (2010). Theory of phononic gaps induced by inertial amplification in finite structures. *Physics Letters A*, *374*(34), 3576–3584. https://doi.org/10.1016/j.physleta.2010.07.001

Yilmaz, C., & Hulbert, G. M. (2017). Dynamics of locally resonant and inertially amplified lattice materials. *Dynamics of Lattice Materials; Phani, AS, Hussein, MI, Eds*, 233.

Yilmaz, C., Hulbert, G. M., & Kikuchi, N. (2007). Phononic band gaps induced by inertial amplification in periodic media. *Physical Review B*, *76*(5), 054309. https://doi.org/10.1103/PhysRevB.76.054309

Yuan, S., Sun, Y., Wang, M., Ding, J., Zhao, J., Huang, Y., Peng, Y., Xie, S., Luo, J., Pu, H., Liu, F., Bai, L., & Yang, X.-D. (2021). Tunable negative stiffness spring using Maxwell normal stress. *International Journal of Mechanical Sciences*, *193*, 106127. https://doi.org/10.1016/j.ijmecsci.2020.106127

Yuksel, O., & Yilmaz, C. (2015). Shape optimization of phononic band gap structures incorporating inertial amplification mechanisms. *Journal of Sound and Vibration*, *355*, 232–245. https://doi.org/10.1016/j.jsv.2015.06.016

Zhang, R., Zhao, Z., & Dai, K. (2019). Seismic response mitigation of a wind turbine tower using a tuned parallel inerter mass system. *Engineering Structures*, *180*, 29–39. https://doi.org/10.1016/j.engstruct.2018.11.020

Zhang, R., Zhao, Z., & Pan, C. (2018). Influence of mechanical layout of inerter systems on seismic mitigation of storage tanks. *Soil Dynamics and Earthquake Engineering*, *114*, 639–649. https://doi.org/10.1016/j.soildyn.2018.07.036

Zhao, Z., Chen, Q., Zhang, R., Pan, C., & Jiang, Y. (2019). Optimal design of an inerter isolation system considering the soil condition. *Engineering Structures*, *196*, 109324. https://doi.org/10.1016/j.engstruct.2019.109324

Zhao, Z., Chen, Q., Zhang, R., Pan, C., & Jiang, Y. (2020). Energy dissipation mechanism of inerter systems. *International Journal of Mechanical Sciences*, *184*, 105845. https://doi.org/10.1016/j.ijmecsci.2020.105845

Zhao, F., Ji, J., Ye, K., & Luo, Q. (2021). An innovative quasi-zero stiffness isolator with three pairs of oblique springs. *International Journal of Mechanical Sciences*, *192*, 106093. https://doi.org/10.1016/j.ijmecsci.2020.106093

Zhao, Z., Zhang, R., Wierschem, N. E., Jiang, Y., & Pan, C. (2020). Displacement mitigation–oriented design and mechanism for inerter-based isolation system. *Journal of Vibration and Control*, 27(17–18), 1991–2003. https://doi.org/10.1177/1077546320951662

Zheng, Y., Zhang, X., Luo, Y., Yan, B., & Ma, C. (2016). Design and experiment of a high-static–low-dynamic stiffness isolator using a negative stiffness magnetic spring. *Journal of Sound and Vibration*, *360*, 31–52. https://doi.org/10.1016/j.jsv.2015.09.019

Zhou, J., Dou, L., Wang, K., Xu, D., & Ouyang, H. (2019). A nonlinear resonator with inertial amplification for very low-frequency flexural wave attenuations in beams. *Nonlinear Dynamics*, *96*(1), 647–665. https://doi.org/10.1007/s11071-019-04812-1

Appendix A. The coefficients of ζ_b from Equation (40)

$$
\begin{aligned}
A = {} & \begin{matrix}(32\kappa^2{\mu_{bv}}^2+64\kappa{\mu_{bv}}^2+32{\mu_{bv}}^2)\eta_{1,2}^{10}\\ +\begin{pmatrix}-48\kappa^3{\mu_{bv}}^2{\eta_b}^2-144\kappa^2{\mu_{bv}}^2{\eta_b}^2-144\kappa{\mu_{bv}}^2{\eta_b}^2-48\kappa^2{\mu_{bv}}^2\\ -48{\mu_{bv}}^2{\eta_b}^2-48\kappa^2\mu_{bv}-96\kappa{\mu_{bv}}^2-96\kappa\mu_{bv}-48{\mu_{bv}}^2-48\mu_{bv}\end{pmatrix}\eta_{1,2}^{8}\end{matrix}\\
& +\begin{pmatrix}16\kappa^4{\mu_{bv}}^2{\eta_b}^4+64\kappa^3{\mu_{bv}}^2{\eta_b}^4+96\kappa^2{\mu_{bv}}^2{\eta_b}^4+64\kappa^3{\mu_{bv}}^2{\eta_b}^2\\ +64\kappa{\mu_{bv}}^2{\eta_b}^4+32\kappa^3\mu_{bv}{\eta_b}^2+192\kappa^2{\mu_{bv}}^2{\eta_b}^2+16{\mu_{bv}}^2{\eta_b}^4\\ +96\kappa^2\mu_{bv}{\eta_b}^2+192\kappa{\mu_{bv}}^2{\eta_b}^2+16\kappa^2{\mu_{bv}}^2\\ +96\kappa\mu_{bv}{\eta_b}^2+64{\mu_{bv}}^2{\eta_b}^2+32\kappa^2\mu_{bv}+32\kappa{\mu_{bv}}^2\\ +32\mu_{bv}{\eta_b}^2+16\kappa^2+64\kappa\mu_{bv}+16{\mu_{bv}}^2+32\kappa+32\mu_{bv}+16\end{pmatrix}\eta_{1,2}^{6}\\
& +\begin{pmatrix}-16\kappa^4{\mu_{bv}}^2{\eta_b}^4-64\kappa^3{\mu_{bv}}^2{\eta_b}^4-96\kappa^2{\mu_{bv}}^2{\eta_b}^4-16\kappa^3{\mu_{bv}}^2{\eta_b}^2\\ -64\kappa{\mu_{bv}}^2{\eta_b}^4-16\kappa^3\mu_{bv}{\eta_b}^2-48\kappa^2{\mu_{bv}}^2{\eta_b}^2-16\mu_{bv}^2{\eta_b}^4\\ -48\kappa^2\mu_{bv}{\eta_b}^2-48\kappa{\mu_{bv}}^2{\eta_b}^2-48\kappa\mu_{bv}{\eta_b}^2-16{\mu_{bv}}^2{\eta_b}^2\\ -16\mu_{bv}{\eta_b}^2\end{pmatrix}\eta_{1,2}^{4}
\end{aligned}
\tag{A.1}
$$

$$
\begin{aligned}
B = {} & \begin{matrix}(6\kappa^4{\mu_{bv}}^2{\eta_b}^2+12\kappa^3{\mu_{bv}}^2{\eta_b}^2+16\kappa^2{\mu_{bv}}^2{\eta_b}^2)\eta_{1,2}^{8}\\ +\begin{pmatrix}-8\kappa^4{\mu_{bv}}^2{\eta_b}^4-32\kappa^3{\mu_{bv}}^2{\eta_b}^4-8\kappa^4{\mu_{bv}}^2{\eta_b}^2-24\kappa^2{\mu_{bv}}^2{\eta_b}^4\\ -8\kappa^4\mu_{bv}{\eta_b}^2-16\kappa^3{\mu_{bv}}^2{\eta_b}^2-16\kappa^3\mu_{bv}{\eta_b}^2-24\kappa^2{\mu_{bv}}^2{\eta_b}^2\\ -24\kappa^2\mu_{bv}{\eta_b}^2\end{pmatrix}\eta_{1,2}^{6}\end{matrix}\\
& +\begin{pmatrix}8\kappa^4{\mu_{bv}}^2{\eta_b}^6+16\kappa^3{\mu_{bv}}^2{\eta_b}^6+8\kappa^4{\mu_{bv}}^2{\eta_b}^4+8\kappa^2{\mu_{bv}}^2{\eta_b}^6\\ +4\kappa^4\mu_{bv}{\eta_b}^4+40\kappa^3{\mu_{bv}}^2{\eta_b}^4+2\kappa^4{\mu_{bv}}^2{\eta_b}^2+20\kappa^3\mu_{bv}{\eta_b}^4\\ +32\kappa^2{\mu_{bv}}^2{\eta_b}^4+4\kappa^4\mu_{bv}{\eta_b}^2+4\kappa^3{\mu_{bv}}^2{\eta_b}^2\\ +16\kappa^2\mu_{bv}{\eta_b}^4+2\kappa^4{\eta_b}^2+8\kappa^3\mu_{bv}{\eta_b}^2\\ +8\kappa^2{\mu_{bv}}^2{\eta_b}^2+4\kappa^3{\eta_b}^2+16\kappa^2\mu_{bv}{\eta_b}^2+8\kappa^2{\eta_b}^2\end{pmatrix}\eta_{1,2}^{4}\\
& +\begin{pmatrix}-8\kappa^4{\mu_{bv}}^2{\eta_b}^6-16\kappa^3{\mu_{bv}}^2{\eta_b}^6-8\kappa^2{\mu_{bv}}^2{\eta_b}^6-8\kappa^3{\mu_{bv}}^2{\eta_b}^4\\ -8\kappa^3\mu_{bv}{\eta_b}^4-8\kappa^2{\mu_{bv}}^2{\eta_b}^4-8\kappa^2\mu_{bv}{\eta_b}^4\end{pmatrix}\eta_{1,2}^{2}
\end{aligned}
\tag{A.2}
$$

$$
\begin{aligned}
C = {} & \begin{matrix}2\kappa^4{\mu_{bv}}^2{\eta_b}^4\eta_{1,2}^{6}\\ +(-3\kappa^4{\mu_{bv}}^2{\eta_b}^6-3\kappa^4{\mu_{bv}}^2{\eta_b}^4-3\kappa^4\mu_{bv}{\eta_b}^4)\eta_{1,2}^{4}\end{matrix}\\
& +\begin{pmatrix}\kappa^4{\mu_{bv}}^2{\eta_b}^8+4\kappa^4{\mu_{bv}}^2{\eta_b}^6+2\kappa^4\mu_{bv}{\eta_b}^6\\ +\kappa^4{\mu_{bv}}^2{\eta_b}^4+2\kappa^4\mu_{bv}{\eta_b}^4+\kappa^4{\eta_b}^4\\ -\kappa^4{\mu_{bv}}^2{\eta_b}^8-\kappa^4{\mu_{bv}}^2{\eta_b}^6-\kappa^4\mu_{bv}{\eta_b}^6\end{pmatrix}\eta_{1,2}^{2}
\end{aligned}
\tag{A.3}
$$